Fragility of the Dirac Cone Splitting in Topological Crystalline Insulator Heterostructures

Craig M. Polley,*,[†] Ryszard Buczko,[‡] Alexander Forsman,[§] Piotr Dziawa,[‡] Andrzej Szczerbakow,[‡] Rafał Rechciński,[‡] Bogdan J. Kowalski,[‡] Tomasz Story,[‡] Małgorzata Trzyna,[∥] Marco Bianchi,[⊥] Antonija Grubišić Čabo,[⊥] Philip Hofmann,[⊥] Oscar Tjernberg,[§] and Thiagarajan Balasubramanian[†]

[†]MAX IV Laboratory, Lund University, 221 00 Lund, Sweden

[‡]Institute of Physics, Polish Academy of Sciences, 02-668 Warsaw, Poland

[§]SCI Materials Physics, KTH Royal Institute of Technology, S-164 40 Kista, Sweden

[∥]Center for Microelectronics and Nanotechnology, Rzeszow University, Rejtana 16A, Rzeszow 35-959, Poland

[⊥]Department of Physics and Astronomy, Interdisciplinary Nanoscience Center (iNANO), Aarhus University, 8000 Aarhus C, Denmark

Ⓢ *Supporting Information*

ABSTRACT: The "double Dirac cone" 2D topological interface states found on the (001) faces of topological crystalline insulators such as $Pb_{1−x}Sn_xSe$ feature degeneracies located away from time reversal invariant momenta and are a manifestation of both mirror symmetry protection and valley interactions. Similar shifted degeneracies in 1D interface states have been highlighted as a potential basis for a topological transistor, but realizing such a device will require a detailed understanding of the intervalley physics involved. In addition, the operation of this or similar devices outside of ultrahigh vacuum will require encapsu-

lation, and the consequences of this for the topological interface state must be understood. Here we address both topics for the case of 2D surface states using angle-resolved photoemission spectroscopy. We examine bulk $Pb_{1−x}Sn_xSe(001)$ crystals overgrown with PbSe, realizing trivial/topological heterostructures. We demonstrate that the valley interaction that splits the two Dirac cones at each $\overline{X}$ is extremely sensitive to atomic-scale details of the surface, exhibiting non-monotonic changes as PbSe deposition proceeds. This includes an apparent total collapse of the splitting for sub-monolayer coverage, eliminating the Lifshitz transition. For a large overlayer thickness we observe quantized PbSe states, possibly reflecting a symmetry confinement mechanism at the buried topological interface.

KEYWORDS: *angle-resolved photoemission spectroscopy (ARPES), topological crystalline insulator, topological heterostructure, valley splitting, quantum confinement*
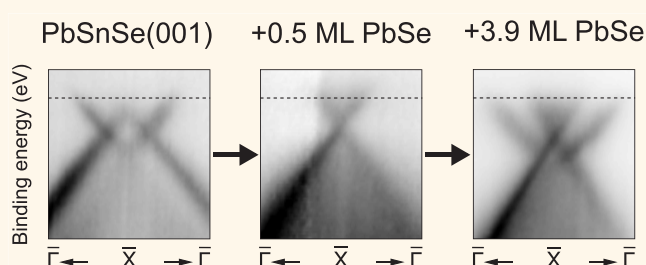
T he recent experimental realization of three-dimensional topological insulators has triggered an expansive program of research, driven largely by the accessibility and rich physics of the 2D electronic states hosted on their surfaces.[1−5] These states are often said to be protected, referencing two distinct concepts. First, the electrical connection of a band-inverted and normal material is not possible without the existence of interface states that thread the bulk band gap. Second, in many band-inverted materials some kind of symmetry exists that forbids hybridization between these cross-gap interface states, thereby ensuring that they remain metallic. These basic characteristics of topological interface states are dictated solely by considerations of

symmetry and bulk band structure and, in the sense that these are not easily affected by perturbations at the surface, can be considered robust.

However, it does not follow that the interface states are immune to surface perturbations. For example, adsorption of nonmagnetic impurities on the topological insulator Bi_2Se_3 surface can dope the surface states.[6−8] Similarly, the topological crystalline insulator (TCI) $Pb_{1−x}Sn_xSe$ can be surface doped with Rb or Sn,[9,10] while lattice distortions that disrupt mirror

symmetry open a band gap.[11,12] For both classes of materials, the surface termination is predicted to play an important role in the topological band dispersions.[13−16]

Details of the interface are also important in special cases where two bulk band inversions project to the same point in the surface Brillouin zone (Figure 1a); that is, they occur at the
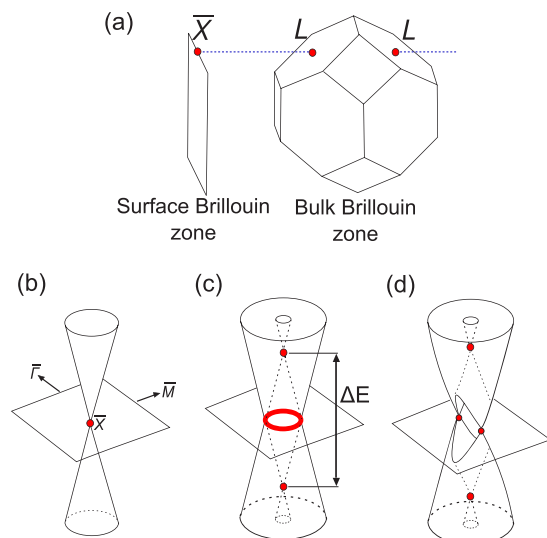

Figure 1. Origin of the double Dirac cone on the $Pb_{1−x}Sn_xSe(001)$ surface. (a) The bulk conduction−valence band inversion occurs at the L points in the bulk Brillouin zone. Two inequivalent L points are located at the same in-plane momentum as the surface $\overline{X}$ point. (b) The resulting topological surface state resembles a Dirac cone with 2-fold valley degeneracy. (c) Intervalley coupling, the focus of this work, splits the degeneracy by ΔE, yielding two Dirac cones that intersect in a circle. (d) Finally, hybridization occurs at all points in the intersection circle except for the two points lying in the mirror symmetry plane along $\overline{\Gamma}− \overline{X}− \overline{\Gamma}$.

same in-plane momentum but different perpendicular momenta. Since it is uncommon for semiconductors to possess a direct band gap away from Γ, this condition is rarely satisfied. To date the only experimentally demonstrated examples are the (001)

faces of (Pb,Sn)Se and (Pb,Sn)Te.[17−19] A simple analysis would suggest that two degenerate Dirac-like surface states would derive from the two bulk band inversions (Figure 1b). In reality the degeneracy is lifted and the resulting band structure features crossings both at $\overline{X}$ and in a ring centered around $\overline{X}$ (Figure 1c). Hybridization eliminates all points of intersection except on the high-symmetry line $\overline{\Gamma}− \overline{X}− \overline{\Gamma}$, where mirror symmetry forbids it. This results in the peculiar band dispersion shown in Figure 1d.

The lifting of degeneracy depicted in Figure 1b (henceforth "valley splitting") is the focus of this study. Valley splitting is an interface effect and cannot be predicted purely from consideration of bulk properties. Symmetry analysis can produce a $k·p$ Hamiltonian that accurately describes the surface band structure;[14,20] however this approach requires empirical tuning and leaves the physical interpretation of the Hamiltonian parameters unclear. Previous experimental studies have observed that the valley splitting depends on the bulk band-inversion magnitude,[21,22,29] but the mechanism remains to be clarified.

Here we demonstrate an alternative approach to studying the valley splitting, in which we grow heterostructures consisting of thin layers of the normal semiconductor PbSe on the TCI $Pb_{0.7}Sn_{0.3}Se$. With angle-resolved photoemission spectroscopy (ARPES) we are able to observe the evolution of the topological interface state as the normal/TCI interface is buried. To date, there are very few spectroscopic studies of buried topological interface states.[23−25] We show that the magnitude of the valley splitting is extremely sensitive to atomic-scale details of the interface and, moreover, is non-monotonic with PbSe thickness (summarized in Figure 2). This evolution can be qualitatively explained with a simple effective mass model, accounting for both our results and those of previous studies. Tight binding calculations elucidate that the valley splitting decays with layer thickness, but in addition is strongly suppressed by PbSe steps at intermediate (noninteger) layer coverage.
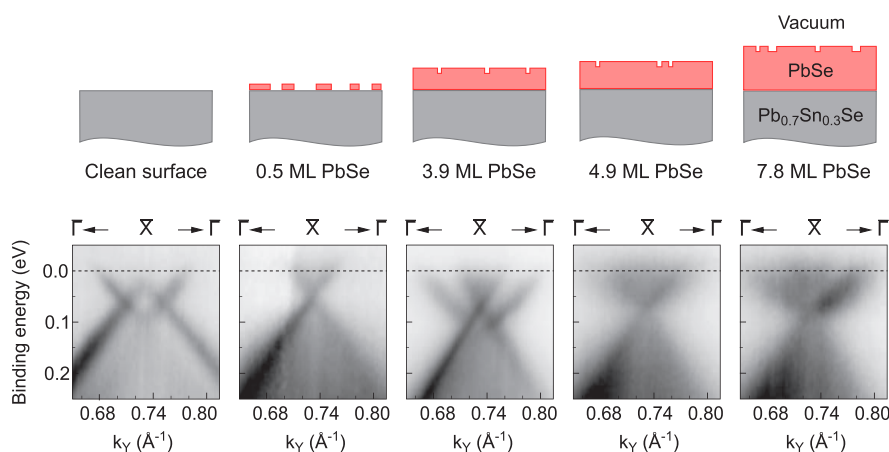

Figure 2. Evolution of valley splitting in a TCI−normal heterostructure. Deposition of PbSe on the TCI $Pb_{1−x}Sn_xSe$ buries the topological−normal interface responsible for the 2D electronic states, but for small thicknesses these states remain accessible to ARPES acquired at a resonant photon energy (18 eV). Sub-monolayer PbSe coverage is sufficient to collapse the valley splitting, while slightly more PbSe recovers it. Non-monotonic splitting can be tracked until blurring from inelastic photoelectron obscures the features of interest for PbSe thicknesses above 8 monolayers.

RESULTS AND DISCUSSION

Physical Depth Profile. Without leaving an ultrahigh vacuum, synchrotron photoemission measurements were performed on the heterostructure samples. Monitoring the intensity ratio of the Sn 4d and Pb 5d core levels (Figure 3a)
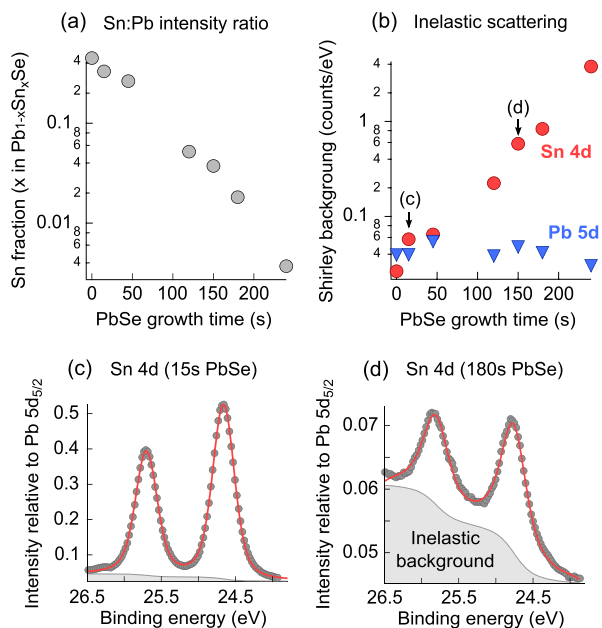

Figure 3. Depth-dependent core level spectroscopy. Monitoring the Pb 5d and Sn 4d core level spectra as a function of PbSe thickness provides important information about the growth. (a) If the Sn is being buried and not segregating, the Sn:Pb intensity ratio should and does exponentially decrease with overlayer thickness (owing to a Beer−Lambert absorption of outgoing photoelectrons). (b) By the same argument, the inelastic background of the Sn 4d should and does increase, while the Pb 5d background remains constant. Analysis details can be found in the Supporting Information. (c, d) Two Sn 4d spectra illustrating both the intensity decrease and scattering increase.

offers an *in situ* estimate of the growth rate, since lead atoms remain at the surface, while tin atoms are buried. As described in the Supporting Information, this method returns a growth rate of ∼0.08 Ås^{-1}. This can be corroborated by *ex situ* measurements: the secondary ion mass spectrometry (SIMS) on the same sample suggests a rate of ∼0.11 Ås^{-1}, while cross sectional electron microscopy of a thick calibration film indicates a growth rate of 0.10 ± 0.01 Ås^{-1} (see Supporting Information). Since electron microscopy is the best calibrated approach, in the remainder of the article we will assume this growth rate when mapping from growth time to film thickness in monolayers (1 ML = 0.306 nm). None of the techniques indicated thickness variation across the sample laterally.

Two important assumptions in these experiments are that the PbSe/Pb$_{0.7}$Sn$_{0.3}$Se interface is sharp and that the band ordering of the PbSe layer is normal. Here the two major concerns are segregation of tin atoms and strain of the PbSe layer, since both could result in a band-inverted PbSe overlayer. Owing to the low growth temperatures, segregation seems unlikely, and indeed the exponentially decreasing core level intensity ratio in Figure 3a suggests that tin atoms remain at the interface. An independent confirmation of this can be obtained from examining the strength of the Shirley background of the

core level spectra (Figure 3b−d). As a function of PbSe thickness, the Pb 5d background is unchanged, while the Sn 4d background increases exponentially. This is consistent with the Sn atoms remaining buried at the interface, resulting in increased scattering of the photoelectrons as they travel to the surface. From our measurements it is not possible to evaluate strain in the PbSe layer. The lattice constant of Pb$_{0.7}$Sn$_{0.3}$Se (a = 6.08 Å) is slightly smaller than that of PbSe (a = 6.12 Å), but the thermal expansion coefficients are essentially identical. Hence if no relaxation occurs during growth, biaxial compressive strain of at most 0.7% could be expected. Previous calculations[26,27] predict that PbSe requires compressive strain of approximately 2% in order to close the band gap. We might therefore expect the PbSe band gap to be reduced, but not closed and certainly not inverted. Due to this low level of strain and film thicknesses below 10 nm, we also do not expect the periodic dislocation network seen previously in STM experiments on IV−VI heterostructures with larger lattice mismatches (>3%).[28,29]

Band Structure Measurements. In Figure 4 we show ARPES data sets measured at three different PbSe overlayer thicknesses. The clean surface (Figure 4a−c) shows the well-known double Dirac cone structure, where the energy splitting of two "parent" Dirac cones results in the emergence of two momentum split "child" Dirac points away from $\overline{X}$. After adding only 0.5 ML of PbSe, the valley splitting of the parent Dirac cones collapses (Figure 4d−f), taking with it the characteristic Lifshitz transition and associated van Hove singularities. When an additional 3.4 ML are deposited, the splitting returns (Figure 4g−i). Note that the constant energy surfaces in Figure 4h clearly indicate two Dirac points, excluding the possibility that this is a single Dirac cone plus a trivial parabolic conduction band state. Careful inspection reveals that the $k_{\parallel}$ dispersion has also changed; the simple $k \cdot p$ model of Liu[14] includes such behavior provided we include higher order terms (discussed in the Supporting Information). Beyond this thickness the splitting appears to collapse once more, although it becomes difficult to be certain owing to the unavoidable increase in blurring of the spectra from inelastic photoelectron scattering. Several additional growth experiments, summarized in Supporting Information, show a similar evolution. The striking changes in the surface state dispersion with increasing PbSe thickness constitute the key result of this study, and the discussion that follows is directed at understanding the origin of this behavior.

The choice of 18 eV as photon energy for the ARPES measurements is significant, partially for high momentum resolution but primarily due to a strong resonant enhancement of the interface state at this energy (also seen on the (111)-oriented surface[50]). The inelastic mean free path for photoelectrons is very short at this energy (<2 nm), and we are attempting to measure electronic states localized to a buried interface. However, the combination of the exponential decay of the interface state wave function toward the surface, the very strong intensity enhancement at $h\nu$ = 18 eV, and the high photon flux available from a synchrotron source means that the topological interface state can indeed be observed for PbSe layer thicknesses up to at least 8 ML (2.5 nm). A similar approach has enabled the measurement of buried dopant layers in silicon.[30,42]

Thickness-Dependent Energy Splitting. To understand the Dirac cone splitting, useful comparisons may be drawn with the valley splitting of quantum well states hosted by semiconductors such as Si,[31,32] Ge,[33] and AlSb.[34] The effective
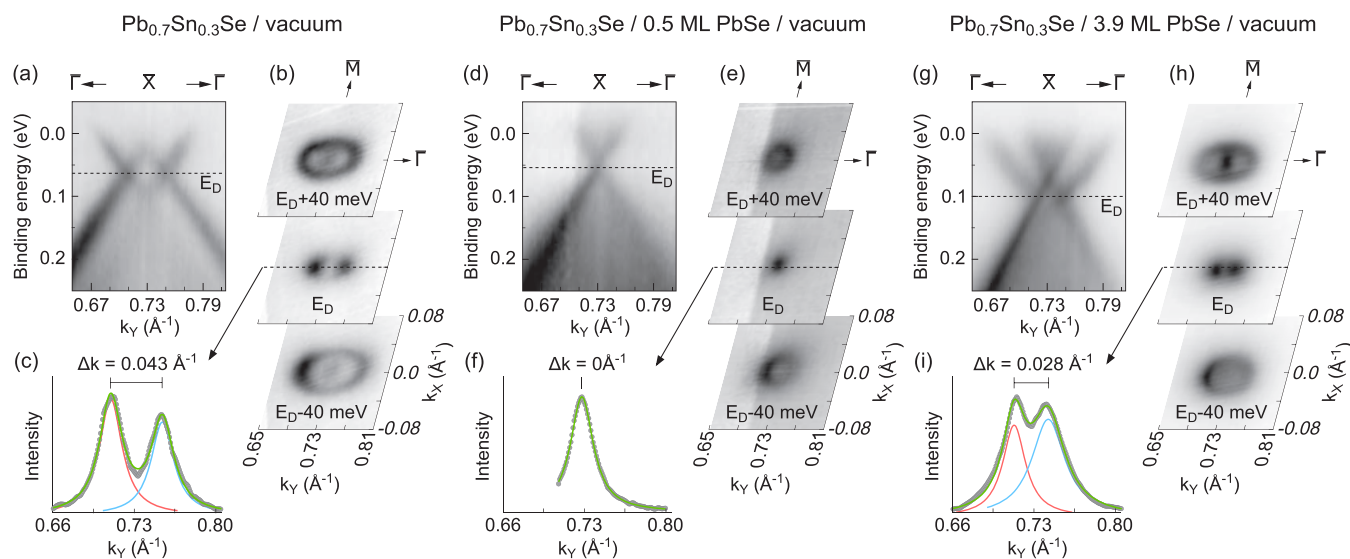
Figure 4. Momentum-resolved spectra of the evolving TCI−normal interface state. The dispersions for (a−c) the clean vacuum/Pb$_{0.7}$Sn$_{0.3}$Se, (d−f) the same after depositing 0.5 ML of PbSe, and (g−i) after depositing a further 3.4 ML of PbSe. Constant energy cuts (b, e, h) clearly demonstrate the varying momentum splitting of the child Dirac points, a direct consequence of the varying energy splitting of the parent Dirac cones. Momentum distribution curves through the child Dirac points (c, f, i) quantify the momentum splitting for the three thickness steps. The stepwise change in intensity in (d) and (e) is an intensity normalization artifact and is the reason for the truncation in (f).

mass approximation (EMA) is a useful framework here. Under the EMA, eigenstates of a confinement potential at a given momentum are constructed from a basis of all bulk Bloch states with the same in-plane momentum but various perpendicular momenta. The resulting wave function can be approximated by a simple envelope function, abstracting away the lattice potential and reducing the problem to that of a simpler quantum mechanical "particle in a box" solution to the bare confinement potential. Several authors have demonstrated that the EMA remains valid with a two-valley bulk basis,[34−38] in which case two degenerate eigenstates are predicted. However, experimentally it has long been known that the degeneracy is usually lifted.[31] The reason is that the two eigenstates will be built from the bulk basis such that they have the same envelope function but differing phases of the underlying Bloch-like oscillation. In free space this has no consequence, but in the presence of a confinement or interface potential the energy eigenvalues slightly differ. In this way the situation is closely analogous to the opening of band gaps at zone boundaries in the nearly free-electron model.

Accurately calculating the splitting magnitude is challenging, but certain qualitative aspects are universally agreed on. The magnitude of the splitting is typically small, but increases rapidly with the strength of the confinement potential. It also oscillates as the width of the confinement potential changes on an atomic scale,[34,36,38−40,43] reflecting the phase difference between the two eigenstates. Finally, and for similar reasons, the presence of disorder or steps can strongly suppress valley splitting.[32,41]

The physics described here is independent of the material system or the origin of the confinement potential. It applies to the two-dimensional states formed by electrostatic band bending in field effect transistor inversion layers, semiconductor heterostructures, and delta-doping profiles, but also to the mass inversions at the boundaries of topological insulators. However, certain properties are unique to band-inverted heterostructures. The wave function is peaked at the well walls rather than inside

the well, with an envelope function that decays exponentially as[5]

$$\phi(z) = A e^{-\frac{|E_g|}{2v} z} \tag{1}$$

where A is a scalar normalization factor, E_g the bulk band gap, and v the bulk band velocity in the z direction. Hence to influence the real-space confinement of the wave function, it is the magnitude and abruptness of the *band inversion* that must be tuned. In contrast to regular quantum wells, electric fields are ineffective to tune the envelope function, since this moves the energy positions of valence and conduction bands equally. This can already be seen in the results of previous studies: electrostatic surface doping of (Pb,Sn)Se causes a rigid energy shift but has no effect on the valley splitting,[9,10] while increasing the band-inversion strength in the bulk by altering composition, temperature or strain increases the valley splitting.[21,22,29] The latter case can be interpreted as pushing the surface state wave function toward the strong potential gradient at the TCI−vacuum interface, thus making the effect of the phase difference more pronounced.

In Figure 5a,b we sketch the situation for Pb$_{0.7}$Sn$_{0.3}$Se with a PbSe overlayer. Considering eq 1 in the limit of a clean surface, the envelope function decays slowly into the Pb$_{0.7}$Sn$_{0.3}$Se but abruptly into the vacuum, since the vacuum can be considered equivalent to a trivial insulator with an infinite band gap. In contrast, PbSe is a finite gap trivial insulator and establishes a slower, piecewise decay of the envelope on the trivial side (Figure 5b). As the thickness of the PbSe layer increases, the interface state wave function grows wider and the envelope amplitude at both the PbSe/(Pb,Sn)Se and vacuum/PbSe interfaces decreases. In line with the preceding discussion, we should expect this to result in an overall decrease of the valley splitting, accompanied by two-monolayer periodic oscillations. Tight binding calculations of PbSe/Pb$_{0.7}$Sn$_{0.3}$Se heterostructures make a similar prediction. Figure 5c plots the surface spectral function for a 16 ML thick PbSe overlayer on Pb$_{0.7}$Sn$_{0.3}$Se(001) and demonstrates a small energy splitting.
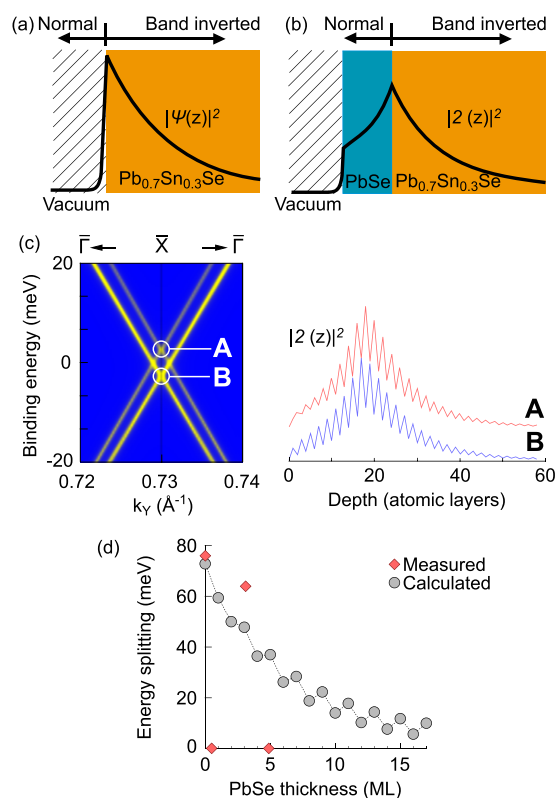
Figure 5. Origin of valley splitting. Sketches of the interface state wave function envelope in the case of (a) a vacuum/$Pb_{0.7}Sn_{0.3}Se$ structure and (b) a vacuum/PbSe/$Pb_{0.7}Sn_{0.3}Se$ heterostructure. Since PbSe has normal band ordering with a finite band gap, it serves to slow the wave function decay on the normal side. Tight binding calculations (c) confirm the overall shape of the wave function envelope, as well as the differing phases of the fast oscillations that are responsible for the valley splitting. Extended calculations as a function of the PbSe overlayer thickness (d, gray circles) confirm an overall decay of the valley splitting modulated by rapid oscillations. Experimental measurements (d, red diamonds) however show a much stronger dependence on thickness.

The depth-resolved probability densities at $k_\| = \bar{X}$ are in agreement with the preceding discussion, with envelope amplitudes peaked at the PbSe/$Pb_{0.7}Sn_{0.3}Se$ interface and decaying exponentially on either side. The antiphase of the underlying fast oscillations is also apparent. Performing the same calculations as a function of PbSe thickness yields the expected depth-dependent reduction in splitting shown in Figure 5d (gray circles).

However, when these calculations are compared with our experimental results (Figure 5d, red diamonds), it is clear that we observe much larger changes in energy splitting. In particular, without even a full monolayer coverage of PbSe the experimental splitting has apparently completely collapsed. This can be accounted for by considering the additional influence of terraces for noninteger layer coverage.

Role of Atomic Terraces. Additional tight binding calculations (Figure 6) illustrate the pronounced effect of surface terraces for the case of partial PbSe coverage. This is achieved by constructing an in-plane structure of 31 atom wide PbSe terraces, aligned in the [110] direction and separated by 19 atoms. This coverage corresponds to 0.62 ML, approximately matching the collapsed Dirac cones in Figure 4d−f. For
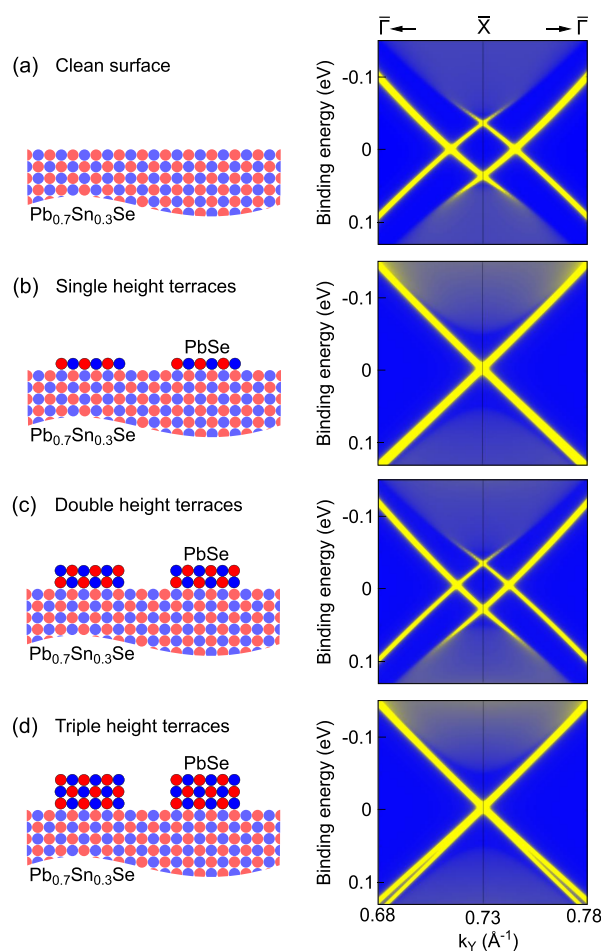

Figure 6. Influence of atomic terraces. Surface spectral functions in the presence of a regular array of atomic terraces, corresponding to incomplete layer coverage. The calculations use terraces 31 atoms wide with a 50 atom period and aligned along the [110] direction. Terraces with odd atomic heights (b, d) strongly suppress the valley splitting due to the resulting phase difference between the two eigenstates. Even height terraces (c) recover nearly the same splitting as the flat surface (a).

odd height terraces there is an almost complete collapse of the splitting, while for even height terraces the splitting is largely unaffected. This is a direct consequence of the antiphase of the two eigenstates, as we discuss in detail in the Supporting Information. In simple terms if the eigenstates are in antiphase, a shift of the surface position equivalent to a π phase shift should exchange bonding and antibonding states. For IV−VI films this occurs every atomic layer. As a result, if the surface is half covered by monatomic terraces, then any fixed phase configuration will integrate to zero splitting.

Several authors have studied cleaved surfaces of (Pb,Sn)Se with ARPES.[9,10,12,17,21,55] After accounting for differences in composition and temperature, the dispersion of the Dirac-like states is quite consistent. Scanning tunneling microscopy observations show that these cleaved surfaces consist of atomically flat terraces separated by 50−100 nm.[45,48] Since a typical ARPES light spot is on the order of 10 μm × 10 μm, it is interesting to consider why atomic steps do not influence the valley splitting of cleaved surfaces but only our PbSe overgrown surfaces. In Figure 7a we summarize tight binding calculations for a $Pb_{0.7}Sn_{0.3}Se$ surface with 0.5 ML terrace coverage, where the lateral size of the terraces are varied (Figure 7a). Note that
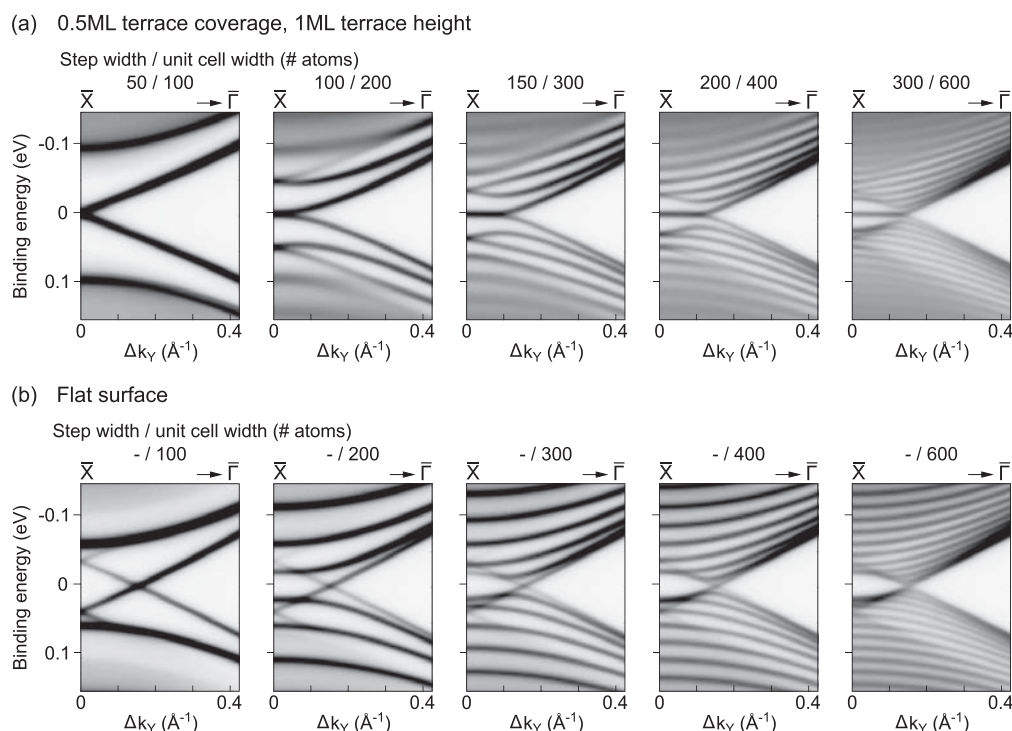
E

(a)   0.5ML terrace coverage, 1ML terrace height

(b)   Flat surface

Figure 7. Size dependence of splitting cancellation. Spectral density functions for a $Pb_{0.7}Sn_{0.3}Se$ surface with 0.5 ML coverage of $Pb_{0.7}Sn_{0.3}Se$ terraces aligned along the $[110]$ direction. For sufficiently large terrace sizes the splitting cancellation no longer occurs (a). Repeating the calculations with a flat surface (b) illustrates the contribution of band-folding due to the increasingly large unit cell. Note that for compactness only $\overline{X}-\overline{\Gamma}$ sections are plotted here as opposed to $\overline{\Gamma}-\overline{X}-\overline{\Gamma}$, such that only one cone is visible.

this is a homostructure, not PbSe terraces on $Pb_{0.7}Sn_{0.3}Se$. We anticipate similar results in both cases.

Figure 7a reveals a size dependence of the splitting cancellation: for narrow terraces (≤100 atomic rows, or 21 nm) the valley splitting has collapsed. For wider terraces the splitting is restored, together with a flat band connecting the two Dirac points. The 1D edge state was recently studied by Sessi *et al.*[45] For comparison, Figure 7b shows flat surfaces with the same unit cell sizes as in Figure 7a. This comparison demonstrates that the many bands appearing in Figure 7 are due to a band-folding artifact from the large unit cells. After unfolding the bands only one Dirac cone would be observed in each panel.

In the effective mass model for valley splitting (see Supporting Information) it is assumed that the wave function phase is fixed throughout the entire region of interest, in which case a surface half covered by π phase shifting terraces should integrate to zero splitting. If the terrace separation is sufficiently large, the assumption of a fixed phase is no longer valid; that is, the wave function phase is able to adjust between terraces. This is the reason that the 1D edge state and the collapse of the Dirac cone splitting cannot occur simultaneously: the former results from the π wave function phase difference at the boundaries of odd-height steps, while the latter occurs only when the wave function phases are unable to make a π phase adjustment between surface steps.

Since cleaved surfaces consist primarily of large terrace widths of 50−100 nm (230−465 atoms), the valley splitting is unaffected. For the PbSe overgrown surfaces studied here we expect a much higher terrace density. The small lattice mismatch between the (Pb,Sn)Se substrate and the PbSe layer should result in pseudomorphic growth. Meanwhile the very low growth temperature (close to room temperature)

should suppress adatom mobility, causing layer-by-layer growth initiated at many disconnected islands. Previous work on IV−VI MBE on lead-salt substrates has demonstrated clear oscillations in reflection high-energy electron diffraction (RHEED) down to the lowest studied substrate temperature of 70 °C, a clear indication of a layer-by-layer growth mode.[44]

We thus believe that a dense network of odd-height atomic steps is reponsible for causing the valley splitting collapse and that these arise due to the low-temperature, layer-by-layer partial filling of the large, atomically flat terraces on the cleaved substrate crystal. Such a growth mode would result in both a uniform height distribution and the necessary higher lateral density of steps compared with the cleaved substrate. Future studies combining topographic measurements (*e.g.*, scanning tunnelling microscopy or atomic force microscopy) with ARPES would be valuable to confirm this.

Finally we comment on a potential implication of our observations. Previous studies[46,47] have highlighted that 1D edge states in thin (001) oriented films of (Pb,Sn)Se also exhibit degeneracies shifted away from time reversal invariant momenta and that this could be exploited for electronic devices. Since mirror symmetry can easily be broken by applying an electric field, an electrostatic gate could open a gap at the Fermi level. Our measurements highlight that while the interface degeneracies are robust, the valley interactions responsible for shifting them away from time reversal invariant momenta is fragile and depends sensitively on the atomic-scale condition of the surface. Presumably the same is true of the condition of edges in films. Without these valley interactions, all degeneracies occur as Kramers doublets. Although the remaining degeneracies would not be topologically protected if mirror symmetry were broken (owing to an even number of band inversions), still a substantial rearrangement of the bands

would be required to eliminate all Fermi level crossings. It is not clear that the electric field produced by a gate electrode could accomplish this, in which case the proposed device would no longer act as a switch. Atomic-scale control of interfaces is fortunately within the capabilities of modern fabrication techniques and may prove necessary to realize these device concepts.

Quantized PbSe States. Finally, we examine the outcome when thicker layers of PbSe are grown, shown in Figure 8. With
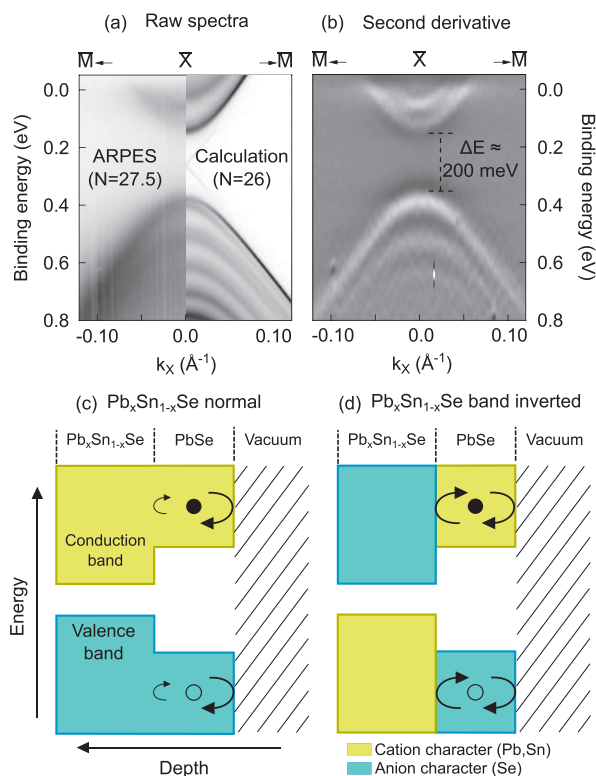

Figure 8. Subband resonances in the thick film limit. With 27.5 ML of PbSe, the topological interface states are no longer observed. Instead the band structure (a) resembles that of bulk PbSe, including a band gap of ΔE = 200 meV. (b) A second derivative image corresponding to (a) highlights the existence of subband resonances in the conduction and valence band. When the substrate is band inverted, reflection of carriers at the PbSe/Pb$_{0.7}$Sn$_{0.3}$Se interface is enhanced due to the differing orbital character (c, d).

27.5 ML (8.4 nm), the topological interface states are now buried beyond the probing depth of UV photoemission. As anticipated, the ARPES spectrum now resembles that of trivial PbSe at ∼130 K, including a 200 meV band gap.[21] Careful inspection reveals subband resonances in both the valence and conduction bands, made clearer in a smoothed second-derivative image (Figure 8b). Spectral density calculations for a similar PbSe overlayer thickness (Figure 8a, right-hand side) reproduce these resonances.

Given that the Pb$_{0.7}$Sn$_{0.3}$Se substrate has a smaller band gap (∼50 meV[21]), a band alignment such as that sketched in Figure 8c would not suggest strong confinement. However, carriers in the PbSe layer still experience partial quantum mechanical reflection from the potential step at the PbSe/Pb$_{0.7}$Sn$_{0.3}$Se interface. The subband resonances would become more pronounced if the substrate were band inverted, as depicted

in Figure 8d and corresponding to the spectra in Figure 8a,b. Now the anion/cation orbital character of the bands is reversed,[27] and reflection of carriers at the interface is greatly enhanced (recall that the topological interface state exists because the two materials cannot otherwise electronically couple). This effect should be generic to any topological insulator/normal heterostructure with a sufficiently thin normal layer and localized in momentum space to the vicinity of the band inversion. An immediate testable implication is that the subband resonances should be weakened by restoring a normal band ordering in the substrate, for example by applying heat or tensile strain. In this way, studying quantization in the overlayer may offer a remote probe of the buried topological interface.

CONCLUSIONS

In summary, by growing thin epitaxial films of the normal semiconductor PbSe on the TCI Pb$_{0.7}$Sn$_{0.3}$Se and studying these *in situ* with ARPES, we have gained a number of important insights. We have shown that the topological interface state is preserved when encapsulated in a heterostructure and that ARPES observations of these buried interface states remain possible at depths of at least 8 ML. The valley splitting responsible for the "double Dirac cone" band dispersion is less robust, to the extent that the splitting can be eliminated by noninteger PbSe layer coverage. All of these findings have important implications for future efforts to build electronic devices from topological crystalline insulator materials. Our observations are also relevant as experimental manifestations of valley splitting, a phenomenon that is crucial to the coherent operation of spin-based solid state quantum computer schemes in multivalley hosts such as Ge and Si.[32,41] Finally, we have observed quantized PbSe subbands for a layer thickness of 8.4 nm and propose that this involves contributions from a type of symmetry confinement. Taken together, our experiments demonstrate that the approach of growing normal overlayers on topological substrates, to date largely unexplored, exposes a wide range of phenomena for further study.

METHODS

Heterostructure Fabrication. The substrates for these experiments were single-crystal Pb$_{0.7}$Sn$_{0.3}$Se, grown *ex situ* by the self-selecting vapor-growth method[49] and cleaved in ultrahigh vacuum to expose a clean (001) surface. All ARPES measurements were performed at a sample temperature of ∼130 K, bringing the substrates well into the TCI phase. For PbSe growth the samples were allowed to warm to room temperature, after which PbSe was deposited *in situ* by an effusion cell loaded with single-crystal PbSe, similar to a previously described arrangement.[50] Since PbSe evaporates molecularly,[51] stoichiometry is expected to be preserved in the grown layers. Substrates were not purposely heated during or after growth, but experienced radiative heating from the effusion cell. Low-energy electron diffraction measurements confirmed that the PbSe overlayer retained the (001) orientation of the substrate, with no indication of a reconstruction. Despite the lack of substrate heating, the PbSe layers remained epitaxial and of relatively good quality, as demonstrated by the well-defined band structures in Figures 4 and 8.

Photoemission Measurements. Photoemission measurements were performed at the I4 beamline in the MAX-IV synchrotron facility,[52] using 18 eV (ARPES) or 90 eV (core level spectroscopy) p-polarized photons. The sample temperature was maintained at ∼130 K during measurements. For the ARPES spectra the total energy resolution was approximately 25 meV, with crystal momentum resolution better than 0.02 Å^{-1}. Additional measurements were

performed at the SGM-3 beamline in the ASTRID 2 synchrotron facility; these are described in the Supporting Information.

Tight Binding Calculations. We employ a nearest neighbor 18-orbital sp^3d^5 model, with PbSe parameters taken from Lent *et al.*[53] For $Pb_{0.7}Sn_{0.3}Se$ we have applied the virtual crystal approximation and SnSe parametrization described previously.[54] We assume that the temperature dependence is dominated by the change of the lattice constant a_0 and rescale our parametrization according to the Harrison rules.[55] Similarly, biaxial strain is treated by rescaling hopping parameters such that the change in energy gap with strain is in agreement with the experimentally determined deformation potential[56] and elastic constants.[57] The spectral densities projected on specific atomic layers have been calculated with the use of a tight binding Hamiltonian for a semi-infinite system and an appropriate modification of a recursive Green's function method described by Lopez Sancho.[58]

ASSOCIATED CONTENT

ⓢ Supporting Information

The Supporting Information is available free of charge on the ACS Publications website at DOI: 10.1021/acsnano.7b07502.

Details of Dirac point valley splitting in the effective mass model, additional photoemission measurements, fitting of the ARPES spectra to a $k \cdot p$ model, details of core level photoemission analysis, *ex situ* cross sectional electron microscopy, and secondary ion mass spectrometry (PDF)

AUTHOR INFORMATION

Corresponding Author
*E-mail: craig.polley@gmail.com.

ORCID ⓞ
Craig M. Polley: 0000-0002-9893-2767
Alexander Forsman: 0000-0003-0125-4128

Author Contributions
C.M.P., A.F., M.B, A.G.Č, and T.B. performed the PbSe deposition and photoemission measurements. A.S. grew the single-crystal (Pb,Sn)Se substrates. P.D. and M.T. performed *ex situ* analysis of the samples. R.B. developed the effective mass and tight binding models, and with R.R performed calculations. C.M.P. carried out the data analysis and wrote the manuscript, with input from all authors. All authors contributed to the interpretation.

Notes
The authors declare no competing financial interest.

REFERENCES

(1) Ando, Y. Topological Insulator Materials. *J. Phys. Soc. Jpn.* **2013**, *82*, 102001.
(2) Qi, X.-L.; Zhang, S.-C. Topological Insulators and Superconductors. *Rev. Mod. Phys.* **2011**, *83*, 1057.

(3) Bansil, A.; Lin, H.; Das, T. Colloquium: Topological Band Theory. *Rev. Mod. Phys.* **2016**, *88*, 021004.
(4) Hasan, M. Z.; Kane, C. L. Colloquium: Topological Insulators. *Rev. Mod. Phys.* **2010**, *82*, 3045.
(5) Zhang, F.; Kane, C. L.; Mele, E. J. Surface States of Topological Insulators. *Phys. Rev. B: Condens. Matter Mater. Phys.* **2012**, *86*, 081303.
(6) Benia, H. M.; Lin, C.; Kern, K.; Ast, C. R. Reactive Chemical Doping of the Bi_2Se_3 Topological Insulator. *Phys. Rev. Lett.* **2011**, *107*, 177602.
(7) Bianchi, M.; Guan, D.; Bao, S.; Mi, J.; Brummerstedt Iversen, B.; King, P. D. C.; Hofmann, P. Coexistence of the Topological State and a Two-Dimensional Electron Gas on the Surface of Bi_2Se_3. *Nat. Commun.* **2010**, *1*, 128.
(8) Valla, T.; Pan, Z.-H.; Gardner, D.; Lee, Y. S.; Chu, S. Photoemission Spectroscopy of Magnetic and Nonmagnetic Impurities on the Surface of the Bi_2Se_3 Topological Insulator. *Phys. Rev. Lett.* **2012**, *108*, 117601.
(9) Pletikosìc, I.; Gu, G. D.; Valla, T. Inducing a Lifshitz Transition by Extrinsic Doping of Surface Bands in the Topological Crystalline Insulator $Pb_{1-x}Sn_xSe$. *Phys. Rev. Lett.* **2014**, *112*, 146403.
(10) Neupane, M.; Xu, S.-Y.; Sankar, R.; Gibson, Q.; Wang, Y. J.; Belopolski, I.; Alidoust, N.; Bian, G.; Shibayev, P. P.; Sanchez, D. S.; Ohtsubo, Y.; Taleb-Ibrahimi, A.; Basak, S.; Tsai, W.-F.; Lin, H.; Durakiewicz, T.; Cava, R. J.; Bansil, A.; Chou, F. C.; Hasan, M. Z. Topological Phase Diagram and Saddle Point Singularity in a Tunable Topological Crystalline Insulator. *Phys. Rev. B: Condens. Matter Mater. Phys.* **2015**, *92*, 075131.
(11) Zeljkovic, I.; Okada, Y.; Serbyn, M.; Sankar, R.; Walkup, R.; Zhou, W.; Liu, J.; Chang, G.; Wang, Y. J.; Hasan, M. Z.; Chou, F.; Lin, H.; Bansil, A.; Fu, L.; Madhavan, V. Dirac Mass Generation From Crystal Symmetry Breaking on the Surfaces of Topological Crystalline Insulators. *Nat. Mater.* **2015**, *14*, 318−324.
(12) Wojek, B. M.; Berntsen, M. H.; Jonsson, V.; Szczerbakow, A.; Dziawa, P.; Kowalski, B. J.; Story, T.; Tjernberg, O. Direct Observation and Temperature Control of the Surface Dirac Gap in a Topological Crystalline Insulator. *Nat. Commun.* **2015**, *6*, 8463.
(13) Zhu, X.-G.; Hofmann, P. Topological Surface States on $Bi_{1-x}Sb_x$: Dependence on Surface Orientation, Termination and Stability. *Phys. Rev. B: Condens. Matter Mater. Phys.* **2014**, *89*, 125402.
(14) Liu, J.; Duan, W.; Fu, L. Two Types of Surface States in Topological Crystalline Insulators. *Phys. Rev. B: Condens. Matter Mater. Phys.* **2013**, *88*, 241303.
(15) Wang, J.; Liu, J.; Xu, Y.; Wu, J.; Gu, B.-L.; Duan, W. Structural Stability and Topological Surface States of the SnTe(111) Surface. *Phys. Rev. B: Condens. Matter Mater. Phys.* **2014**, *89*, 125308.
(16) Safaei, S.; Kacman, P.; Buczko, R. Topological Crystalline Insulator (Pb,Sn)Te: Surface States and Their Spin Polarization. *Phys. Rev. B: Condens. Matter Mater. Phys.* **2013**, *88*, 045305.
(17) Dziawa, P.; Kowalski, B. J.; Dybko, K.; Buczko, R.; Szczerbakow, A.; Szot, M.; Łusakowska, T.; Balasubramanian, T.; Wojek, B. M.; Berntsen, M. H.; Tjernberg, O.; Story, T. Topological Crystalline Insulator States in $Pb_{1-x}Sn_xSe$. *Nat. Mater.* **2012**, *11*, 1023−1027.
(18) Tanaka, Y.; Ren, Z.; Sato, T.; Nakayama, K.; Souma, S.; Takahashi, T.; Segawa, K.; Ando, Y. Experimental Realization of a Topological Crystalline Insulator in SnTe. *Nat. Phys.* **2012**, *8*, 800−803.
(19) Xu, S.-Y.; Liu, C.; Alidoust, N.; Neupane, M.; Qian, D.; Belopolski, I.; Denlinger, J. D.; Wang, Y. J.; Lin, H.; Wray, L. A.; Landolt, G.; Slomski, B.; Dil, J. H.; Marcinkova, A.; Morosan, E.; Gibson, Q.; Sankar, R.; Chou, F. C.; Cava, R. J.; Bansil, A.; Hasan, M. Z. Observation of a Topological Crystalline Insulator Phase and Topological Phase Transition in $Pb_{1-x}Sn_xTe$. *Nat. Commun.* **2012**, *3*, 1192.
(20) Wang, Y. J.; Tsai, W.-F.; Lin, H.; Xu, S.-Y.; Neupane, M.; Hasan, M. Z.; Bansil, A. Nontrivial Spin Texture of the Dirac Cones on the Surface of Topological Crystalline Insulator SnTe. *Phys. Rev. B: Condens. Matter Mater. Phys.* **2013**, *87*, 235217.
(21) Wojek, B. M.; Dziawa, P.; Kowalski, B. J.; Szczerbakow, A.; Black-Schaffer, A. M.; Berntsen, M. H.; Balasubramanian, T.; Story, T.;

Tjernberg, O. Band Inversion and the Topological Phase Transition in (Pb,Sn)Se. *Phys. Rev. B: Condens. Matter Mater. Phys.* **2014**, *90*, 161202.

(22) Tanaka, Y.; Sato, T.; Nakayama, K.; Souma, S.; Takahashi, T.; Ren, Z.; Novak, M.; Segawa, K.; Ando, Y. Tunability of the k-space Location of the Dirac Cones in the Topological Crystalline Insulator $Pb_{1-x}Sn_xTe$. *Phys. Rev. B: Condens. Matter Mater. Phys.* **2013**, *87*, 155105.

(23) Berntsen, M. H.; Götberg, O.; Wojek, B. M.; Tjernberg, O. Direct Observation of Dirac States at the Interface Between Topological and Normal Insulators. *Phys. Rev. B: Condens. Matter Mater. Phys.* **2013**, *88*, 195132.

(24) Yoshimi, R.; Tsukazaki, A.; Kikutake, K.; Checkelsky, J. G.; Takahashi, K. S.; Kawasaki, M.; Tokura, Y. Dirac Electron States Formed at the Heterointerface Between a Topological Insulator and a Conventional Semiconductor. *Nat. Mater.* **2014**, *13*, 253−257.

(25) Eich, A.; Rollfing, N.; Arnold, F.; Sanders, C.; Ewen, P. R.; Bianchi, M.; Dendzik, M.; Michiardi, M.; Mi, J.-L.; Bremholm, M.; Wegner, D.; Hofmann, P.; Khajetoorians, A. A. Absence of Superconductivity in Ultrathin Layers of FeSe Synthesized on a Topological Insulator. *Phys. Rev. B: Condens. Matter Mater. Phys.* **2016**, *94*, 125437.

(26) Barone, P.; Di Sante, D.; Picozzi, S. Strain Engineering of Topological Properties in Lead-Salt Semiconductors. *Phys. Status Solidi RRL* **2013**, *7*, 1102−1106.

(27) Hsieh, T. H.; Lin, H.; Liu, J.; Duan, W.; Bansil, A.; Fu, L. Topological Crystalline Insulators in the SnTe Material Class. *Nat. Commun.* **2012**, *3*, 982.

(28) Springholz, G.; Wiesauer, K. Nanoscale Dislocation Patterning in PbTe/PbSe(001) Lattice-Mismatched Heteroepitaxy. *Phys. Rev. Lett.* **2001**, *88*, 015507.

(29) Zeljkovic, I.; Walkup, D.; Assaf, B. A.; Scipioni, K. L.; Sankar, R.; Chou, F.; Madhavan, V. Strain Engineering Dirac Surface States in Heteroepitaxial Topological Crystalline Insulator Thin Films. *Nat. Nanotechnol.* **2015**, *10*, 849−853.

(30) Miwa, J. A.; Hofmann, P.; Simmons, M. Y.; Wells, J. W. Direct Measurement of the Band Structure of a Buried Two-Dimensional Electron Gas. *Phys. Rev. Lett.* **2013**, *110*, 136801.

(31) Ando, T.; Fowler, A. B.; Stern, F. Electronic Properties of Two-Dimensional Systems. *Rev. Mod. Phys.* **1982**, *54*, 437.

(32) Zwanenburg, F.; Dzurak, A. S.; Morello, A.; Simmons, M. Y.; Hollenberg, L. C. L.; Klimeck, G.; Rogge, S.; Coppersmith, S. N.; Eriksson, M. A. Silicon Quantum Electronics. *Rev. Mod. Phys.* **2013**, *85*, 961.

(33) Carter, D. J.; Warschkow, O.; Gale, J. D.; Scappucci, G.; Klesse, W. M.; Capellini, G.; Rohl, A. L.; Simmons, M. Y.; McKenzie, D. R.; Marks, N. A. Electronic Structure of Phosphorus and Arsenic δ-Doped Germanium. *Phys. Rev. B: Condens. Matter Mater. Phys.* **2013**, *88*, 115203.

(34) Ting, D. Z.-Y.; Chang, Y.-C. L-Valley-Derived States in (001) GaSb/AlSb Quantum Wells and Superlattices. *Phys. Rev. B: Condens. Matter Mater. Phys.* **1988**, *38*, 3414.

(35) Sham, L. J.; Nakayama, M. Effective-Mass Approximation in the Presence of an Interface. *Phys. Rev. B: Condens. Matter Mater. Phys.* **1979**, *20*, 734.

(36) Valavanis, A.; Ikonić, Z.; Kelsall, R. W. Intervalley Splitting and Intersubband Transitions in n-Type Si/SiGe Quantum Wells: Pseudopotential vs. Effective Mass Calculation. *Phys. Rev. B: Condens. Matter Mater. Phys.* **2007**, *75*, 205332.

(37) Saraiva, A. L.; Calderón, M. J.; Hu, X.; Das Sarma, S.; Koiler, B. Physical Mechanisms of Interface-Mediated Intervalley Coupling in Si. *Phys. Rev. B: Condens. Matter Mater. Phys.* **2009**, *80*, 081305.

(38) Nestoklon, M. O.; Golub, L. E.; Ivchenko, E. L. Spin and Valley-Orbit Splittings in SiGe/Si Heterostructures. *Phys. Rev. B: Condens. Matter Mater. Phys.* **2006**, *73*, 235334.

(39) Boykin, T. B.; Kharche, N.; Klimeck, G. Valley Splitting in Finite Barrier Quantum Wells. *Phys. Rev. B: Condens. Matter Mater. Phys.* **2008**, *77*, 245320.

(40) Virgilio, M.; Grosso, G. Valley Splitting and Optical Intersubband Transitions at Parallel and Normal Incidence in [001]-Ge/SiGe Quantum Wells. *Phys. Rev. B: Condens. Matter Mater. Phys.* **2009**, *79*, 165310.

(41) Goswami, S.; Slinker, K. A.; Friesen, M.; McGuire, L. M.; Truitt, J. L.; Tahan, C.; Klein, L. J.; Chu, J. O.; Mooney, P. M.; van der Weide, D. W.; Joynt, R.; Coppersmith, S. N.; Eriksson, M. A. Controllable Valley Splitting in Silicon Quantum Devices. *Nat. Phys.* **2007**, *3*, 41−45.

(42) Miwa, J. A.; Warschkow, O.; Carter, D. J.; Marks, N. A.; Mazzola, F.; Simmons, M. Y.; Wells, J. W. Valley Splitting in a Silicon Quantum Device Platform. *Nano Lett.* **2014**, *14*, 1515−1519.

(43) Freisen, M.; Chutia, S.; Tahan, C.; Coppersmith, S. N. Valley Splitting Theory of SiGe/Si/SiGe Quantum Wells. *Phys. Rev. B: Condens. Matter Mater. Phys.* **2007**, *75*, 115318.

(44) Springholz, G.; Bauer, G. Low Temperature Growth of PbTe and of PbTe/$Pb_{1-x}Eu_x$Te Multi-Quantum Wells by Molecular Beam Epitaxy. *J. Cryst. Growth* **1994**, *144*, 157−172.

(45) Sessi, P.; Di Sante, D.; Szczerbakow, A.; Glott, F.; Wilfert, S.; Schmidt, H.; Bathon, T.; Dziawa, P.; Greiter, M.; Neupert, T.; Sangiovanni, G.; Story, T.; Thomale, R.; Bode, M. Robust Spin-Polarized Midgap States at Step Edges of Topological Crystalline Insulators. *Science* **2016**, *354*, 1269−1273.

(46) Liu, J.; Hsieh, T. H.; Wei, P.; Moodera, J.; Fu, L. Spin-Filtered Edge States With an Electrically Tunable Gap in a Two-Dimensional Topological Insulator. *Nat. Mater.* **2014**, *13*, 178−183.

(47) Ezawa, M. Electrically Tunable Conductance and Edge Modes in Topological Crystalline Insulator Thin Films: Minimal Tight-Binding Model Analysis. *New J. Phys.* **2014**, *16*, 065015.

(48) Gyenis, A.; Drozdov, I. K.; Nadj-Perge, S.; Jeong, O. B.; Seo, J.; Pletikosič, I.; Valla, T.; Gu, G. D.; Yazdani, A. Quasiparticle Interference on the Surface of the Topological Crystalline Insulator $Pb_{1-x}Sn_x$Se. *Phys. Rev. B: Condens. Matter Mater. Phys.* **2013**, *88*, 125414.

(49) Szczerbakow, A.; Berger, H. Investigation of the Composition of Vapour-Grown $Pb_{1-x}Sn_x$Se Crystals (x ⩽ 0.4) by Means of Lattice Parameter Measurements. *J. Cryst. Growth* **1994**, *139*, 172−178.

(50) Polley, C. M.; Dziawa, P.; Reszka, A.; Szczerbakow, A.; Minikayev, R.; Domagala, J. Z.; Safaei, S.; Kacman, P.; Buczko, R.; Adell, J.; Berntsen, M. H.; Wojek, B. M.; Tjernberg, O.; Kowalski, B. J.; Story, T.; Balasubramanian, T. Observation of Topological Crystalline Insulator Surface States on (111)-Oriented $Pb_{1-x}Sn_x$Se Films. *Phys. Rev. B: Condens. Matter Mater. Phys.* **2014**, *89*, 075317.

(51) Springholz, G.; Bauer, G. Molecular Beam Epitaxy of IV-VI Semiconductor Hetero- and Nano-Structures. *Phys. Status Solidi B* **2007**, *244*, 2752−2767.

(52) Jensen, B. N.; Butorin, S. M.; Kaurila, T.; Nyholm, R.; Johansson, L. I. Design and Performance of a Spherical Grating Monochromator Used at MAX I. *Nucl. Instrum. Methods Phys. Res., Sect. A* **1997**, *394*, 243−250.

(53) Lent, C. S.; Bowen, M. A.; Dow, J. D.; Allgaier, R. S.; Sankey, O. F.; Ho, E. S. Relativistic Empirical Tight-Binding Theory of the Energy Bands of GeTe, SnTe, PbTe, PbSe, PbS, and their Alloys. *Superlattices Microstruct.* **1986**, *2*, 491−499.

(54) Safaei, S.; Galicka, M.; Kacman, P.; Buczko, R. Quantum Spin Hall Effect in IV-VI Topological Crystalline Insulators. *New J. Phys.* **2015**, *17*, 063041.

(55) Wojek, B. M.; Buczko, R.; Safaei, S.; Dziawa, P.; Kowalski, B. J.; Berntsen, M. H.; Balasubramanian, T.; Leandersson, M.; Szczerbakow, A.; Kacman, P.; Story, T.; Tjernberg, O. Spin-Polarized (001) Surface States of the Topological Crystalline Insulator $Pb_{0.73}Sn_{0.27}$Se. *Phys. Rev. B: Condens. Matter Mater. Phys.* **2013**, *87*, 115106.

(56) Simma, M.; Fromherz, T.; Bauer, G.; Springholz, G. Type I/Type II Band Alignment Transition in Strained PbSe/PbEuSeTe Multiquantum Wells. *Appl. Phys. Lett.* **2009**, *95*, 212103.

(57) Lippmann, G.; Kastner, P.; Wanninger, W. Elastic Constants of PbSe. *Phys. Status Solidi A* **1971**, *6*, K159−161.

(58) Lopez Sancho, M. P.; Lopez Sancho, J. M.; Rubio, J. Highly Convergent Schemes for the Calculation of Bulk and Surface Green Functions. *J. Phys. F: Met. Phys.* **1985**, *15*, 851.